Propulsion and Energy Forum
July 28-30, 2014, Cleveland, OH
50th AIAA/ASME/SAE/ASEE Joint Propulsion Conference

Effects of Wall Temperature and Surface Roughness on the Plasma Sheath

Samuel Langendorf[1], Mitchell L. R. Walker[2]
High-Power Electric Propulsion Laboratory, Georgia Institute of Technology
Atlanta, GA 30332 USA

In this experiment, plasma sheath potential profiles are measured over smooth (R_a < 0.2 μm) and rough (R_a = 10.4 μm) wall material samples of AX05-grade boron nitride over the temperature range 0 to 600 °C. Argon plasma with a number density of approximately 3 x 10^{12} m^{-3} is generated at an operating pressure 1.0 x 10^{-4} Torr-Ar using a multidipole-type plasma device. The sheath potential profile at the surface of each sample is measured with emissive probes, and electron number densities and temperatures are measured in the bulk plasma with a planar Langmuir probe. The electron energy distribution of the plasma is non-Maxwellian, with isotropic and directed energetic electron populations from 50 – 200 eV and hot and cold Maxwellian populations from 3.6 – 6.4 eV and 0.3 – 1.3 eV, respectively. Plasma Debye lengths range from 3 to 6 mm and ion-neutral mean free paths are maintained at least two orders of magnitude greater in order to study the collisionless sheath regime. Sheath thicknesses range from approximately 30 to 60 mm, and are smaller in the collapsed sheaths. For both rough and smooth samples, increased primary electron energy is seen to affect a transition in the sheath structure to a collapsed profile. Secondary electron emission (SEE) is inferred as the mechanism for the transition in accordance with prevalent theory. Increased surface roughness causes the sheath to transition at 40 ± 20 eV greater plasma primary electron energies, believed due to decreased SEE from geometrical obstruction of escaping electrons. When rough and smooth wall are in the same sheath regime, the sheaths are similar within ~ 2 V. Elevating the wall material temperature to 600 ºC causes the sheath over the rough sample to collapse at 125 ± 20 eV greater primary electron energy in comparison to the unheated sample, believed due to decreased SEE. The effect of heating to 600 ºC on the smooth sample was much less, causing the sheath to collapse at 10 ± 20 eV greater primary electron energy. These effects may be primarily due to removal of contaminants from the material surface rather than a decoupled effect of wall temperature.

I. Introduction

In order to make the high specific impulse capability of electric propulsion devices available for a wider range of missions and applications, it is necessary to increase their specific thrust and power density beyond current state-of-the-art levels. The plasma-wall interaction is a primary factor limiting increases in power density in propulsion devices, in particular ion losses to the wall. Ideally, the wall will serve only to fix the physical location of the plasma. In reality, the wall absorbs energy from the plasma, exchanges energetic electrons for low energy electrons through secondary electron emission (SEE), neutralizes ions, and introduces undesired sputtered wall material.

The plasma sheath is a non-neutral boundary region that arises between a plasma and wall and governs charged-particle fluxes to and from the wall. In previous work, we have measured plasma sheaths undergoing multiple phenomena of interest in EP devices, such as changes in neutral pressure[1], plasma electron energy distribution, and wall material[2]. In particular, we have observed collapsed sheath potential profiles due to SEE. The occurrence of these collapsed sheaths prompts the question of the specific plasma-and-wall conditions under which they occur, including type of wall material, what wall temperature and what level of surface roughness, which we investigate in the present work. The link between wall material and SEE yield has been experimentally characterized in literature for a variety of materials[3]. Surface roughness in general decreases SEE as it provides geometric obstacles for escaping electrons, however it may also increase SEE due to increasing the effective incidence angle of incident energetic particles[4]. The effect of wall temperature on the sheath is unknown: it could affect the sheath through influencing the temperature of emitted electrons, and also through evaporation of surface contaminants (which are

[1] Graduate Student, School of Aerospace Engineering, 270 Ferst Dr. NW, Student Member AIAA
[2] Associate Professor, School of Aerospace Engineering, 270 Ferst Dr. NW, Associate Fellow AIAA

associated with increased SEE.) In this experiment, we measure sheaths over smooth and rough BN samples at temperatures from 20 to 600 °C.

II. Setup

In this experiment, a multidipole plasma device is used to investigate plasma sheath phenomena. Multidipole devices have been used in many experiments since their invention in the early 1970's as a way to generate quiescent and spatially uniform plasmas[5-8]. The device consists of an electrically grounded cylindrical aluminum cage lined with permanent magnets that confine ionizing electrons generated by emissive filaments within the device. The filaments are biased below ground (and below the resultant bulk plasma potential) to impart energy to the thermionically emitted electrons. Neutral molecules enter the device from the vacuum chamber, which receives mass flow input directed away from the device to allow the gas to expand throughout the chamber and enter the plasma cell with a spatially uniform number density. In this experiment, the gas input into the vacuum chamber is positioned 2 meters from the plasma cell center, aimed at the chamber wall. Figure 1 shows a schematic of the plasma cell, which has been described in detail elsewhere[9].

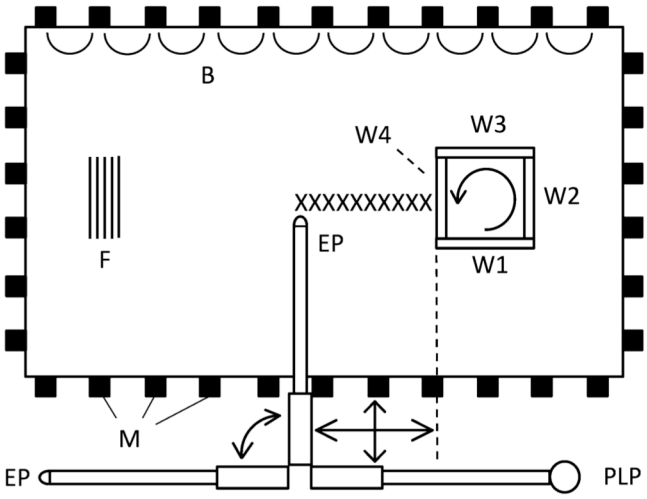

Figure 1. Schematic of experimental layout. *F = filaments, M = magnets, B = nominal magnetic field, LP = Langmuir probe, EP = emissive probe, W = wall material sample, X = nominal data measurement location. Emissive probe orientation rotated 90° in figure to show hairpin tip geometry. Figure not to scale.*

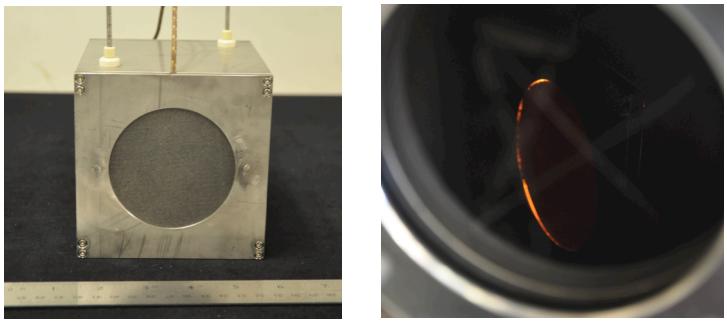

a) **b)**

Figure 2. Wall material sample heater. *a) Heater assembled with placeholder graphite wall material sample. b) Sample heater operating in bell jar.*

The sample heater is a cube fabricated from a sheet of reflective finish 304 stainless steel, shown in Figure 2. The heater is assembled such that the reflective surface faces inward. Radiative heating elements are formed inside the cube by 0.042 inch tantalum wire coiled around 3/8-inch OD alumina tubing. Temperature is monitored using a k-type thermocouple clamped to the interior face of the sample.

The plasma device is operated in the Georgia Institute of Technology Vacuum Test Facility 2, which is 9.2 meters long, 4.9 meters in diameter and uses ten CVI TM1200i cryopumps to achieve a base pressure of 1.9×10^{-9} Torr[10]. In these experiments the plasma device is positioned in the center of the chamber. Only two of the cryopumps are operated during this experiment, in order to decrease pumping speed so that the desired experimental pressures can be obtained using a 500 sccm-N_2 range MKS 1179A01352CS1BV mass flow controller. This mass flow controller is used to flow 99.999% argon into the chamber and control the pressure. Pressure is measured with ± 25% accuracy[11] using a Bayard-Alpert 571 ionization gauge connected to the vacuum chamber with a Varian XGS-600 gauge controller, corrected for argon using a gas correction multiplier of 0.77. For these experiments, the pressure is held constant at 1.0×10^{-4} Torr-Ar, which gives an electron-neutral ionization mean free path of approximately 1.3 meters. Although this is on the same length scale as the plasma device, the electron path length within the device is increased by the confinement added by the cusp-shaped magnetic fields so that enough ionization takes place to create a low-density plasma (~ 10^{13} m^{-3}). The ion-neutral mean free path is 0.8 meters, which is much larger than the sheath thicknesses interrogated (all < 0.1 m) and thus presheath potential fall within the interrogated region is expected to be minimal. Monitoring of vacuum chamber pressure did not show any pressure fluctuations that were visible within the ranged resolution of the ion gauge controller (± 1×10^{-5} Torr-Ar).

The five filaments are resistively heated in parallel with a TDK-Lambda 60V-25A DC power supply electrically isolated from ground by a Stancor GIS-1000 isolation transformer and electrically biased with a Keithley 2410 Sourcemeter. The discharge current is held constant at 10.0 mA in these experiments by manual adjustment of the filament heating current. The nominal value of the filament heating voltage and current is 7.34 V and 10.98 A, though it is adjusted throughout the experiment to account for drift in the discharge current. The discharge current exhibits drift on the order of 0.5 mA over 5 minutes, but this decreases to 0.1 mA over 5 min after approximately 20 minutes of operation at a constant bias voltage. When drift in the discharge current occurs, it is held constant to 10.0 mA by manual hundredth-amp adjustments to the filament heating current.

A. Wall Material Samples

The wall material samples are 3-inch diameter, 0.25-inch thick discs, grade AX05 boron nitride. The smooth samples are polished using a Buehler Metaserv 250 grinder-polisher at 300 rpm, and the roughened samples are abraded with 120 grit SiC polishing paper. The resulting surface finish is characterized using a LEXT OLS4000 profilometer. A representative scan of the roughened sample is shown in Figure 3. The average roughness (computed as the arithmetic mean of the absolute deviations in height from the mean height) is 10.4 μm, averaged across 5 scans at 20x magnification. This is the same order of roughness as has been measured from the wall of an eroded HET channel using the same profilometer[12]. The standard deviation of the average roughness between the five scans is 2.68 μm. The smooth surface had no surface roughness that could be observed within the profilometer resolution of 0.2 μm.

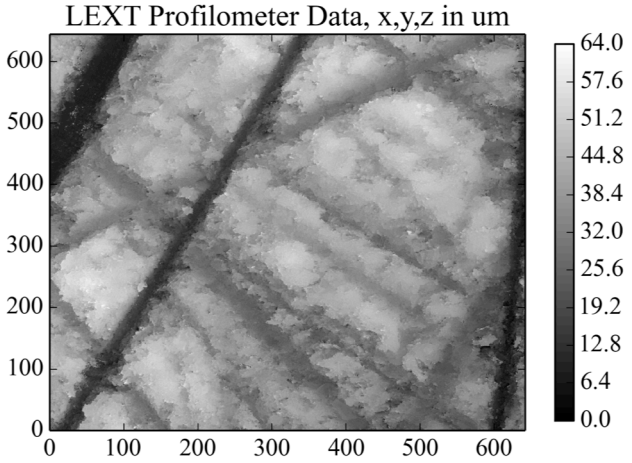

Figure 3. Surface scan of wall material sample. *Scan taken of the roughened AX05 boron nitride wall material sample at 20x magnification. Scores from abrasion treatment are shown. Scanned prior to plasma exposure.*

A cube-shaped stainless steel sample holder is positioned on centerline within the multidipole plasma device and supported on a rotation stage, such that the different samples can be turned to the measurement position (W4 in Figure 1.) The wall material samples are positioned on the horizontal faces of the cube. The metal sample holder is electrically isolated from the plasma device and chamber to avoid giving the plasma electrons an alternative path to ground than the designed path across the cusp magnetic fields.

B. Diagnostics

The sheath potential profile is measured using an emissive probe as shown in Figure 1. A redundant emissive probe and Langmuir probe are included on a rotation stage, so that probe can be changed without breaking vacuum. The emissive probes are constructed of telescoping alumina tubing and a hairpin 0.005-inch diameter thoriated tungsten filament emissive tip. The probe is heated until it has begun to glow in order to clean the probe tip, but only so hot that a small amount (~50 μA) emission current is observed. The plasma potential is determined to be the voltage at which the inflection point of the probe characteristic occurs. This technique sacrifices a small amount of absolute accuracy with respect to the technique of multiple inflection points extrapolated to zero emission and increases noise susceptibility since there are no redundant sweeps[13]. The resultant accuracy is estimated at T_e / 5e, double that of the extrapolated method. With both cold (~ 1 eV) and hot (~ 5 eV) electron populations present in the plasma, the accuracy is estimated at 1 V. It is employed in this experiment because it allows a full sheath measurement to be taken more quickly (3.5 minutes) and decreases potential errors due to drift in the plasma operating condition. The emissive probe is positioned using a Parker 4062000XR linear motion table with a bi-directional repeatability of ±5 μm. The origin of the probe position is defined where the probe support touches the alumina wall, which was determined to within ±125 μm.

Bulk plasma parameters are measured using a planar Langmuir probe positioned in the center of the plasma device. The Langmuir probe is constructed of alumina tubing with a 0.303-inch diameter, 0.020-inch thick tungsten disc tip. Five linear stair sweeps from -200 to 0 V were collected and averaged, with a dwell time of 20 ms at each

voltage and a step interval of 0.2 V. The probe characteristics are corrected for singly-charged argon ion- and electron-induced SEE using data for tungsten from Ref. 14 and Ref. 15 (degassed target), respectively. The probe is cleaned by ion bombardment at -500 V bias for a period of 15 minutes before data collection, after which time no noticeable change is observable in I-V characteristics. The probe is re-cleaned at -500 V for 30 seconds after the collection of each trace. Two traces are collected at each condition to verify that no spurious artifacts are present, and the average of the two traces is used for processing.

C. Langmuir Probe Processing

In order to achieve a low plasma density and prevalent energetic electron populations, the plasma device is operated at a discharge current of 10 mA. The filament bias voltage is varied between -80 and -200 V. The I-V characteristics obtained with the planar Langmuir probe do not show a prevalent 'knee' and saturation of the collected current, and both the electron and ion collection regions show a linear relationship with voltage as typical of the orbital-motion-limited spherical probe. This indicates that the sheath thickness is significantly greater than the probe diffusion length of 3 mm, which is later supported by the emissive probe measurements of the wall material samples.

The Langmuir probe is interpreted in the following steps. An ion density and temperature is assumed to fit the ion collection region of the probe curve according to (1)[16] and the fit ion current is subtracted out.

$$I_i = A_p n_i e \sqrt{\frac{k_B T_i}{2\pi M}} (1 - eV_p / kT_i) \qquad (1)$$

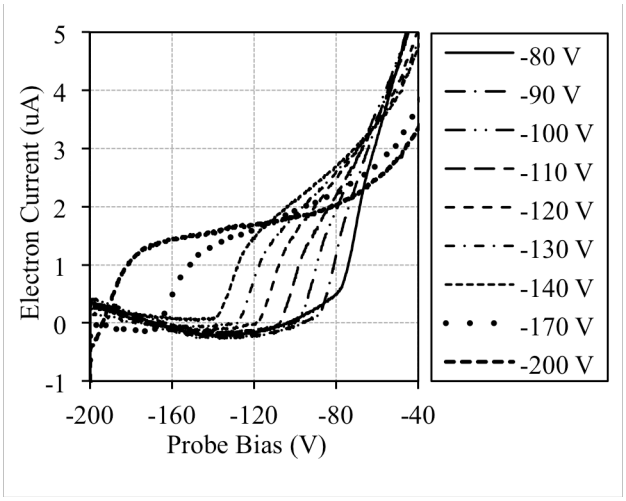

Figure 4. Electron current traces obtained with planar Langmuir probe in the ion-collecting region (after subtraction of ion current.) *Collection of primary electrons is observed when the probe is biased above the discharge filament bias voltage. As the discharge filament is biased to increasingly negative voltages, the primary electron current collection signature changes from linear (isotropic) to step (beam.)*

In equation 1, I_i is the positive ion current collected by the Langmuir probe of area A_p at bias V_p with respect to the plasma potential, n_i and T_i are the ion number density and temperature, and M is the ion mass. After the ion current has been subtracted, the revealed energetic electron current (shown in Figure 4) is observed to be composed of a directed-velocity component and an isotropic component. The directed-velocity component is fit by a uniform distribution spanning the range of primary energies given to the electrons by the voltage drop across the length of the discharge filament. A linear fit is used for the isotropic component, following Hershkowitz et al.[17]. Once the fits have been applied, the energetic electrons are subtracted out as well. The remaining electrons conform well to a bi-Maxwellian distribution as has been observed in multidipole argon plasmas at pressures near 1 x10^{-4} Torr-Ar[18], and fit accordingly. All fits are adjusted self-consistently to reduce error, resulting in a constructed I-V curve that follows the collected data with relative error <1%.

III. Results and Discussion

A. Plasmas

Plasma densities (Figure 6) are measured on the order of 3 x 10^{12} m^{-3}, detecting similar amounts of hot and cold Maxwellian electrons. We agree with the assessment of Robertson et al.[19] that the "hot" population is created and replenished by secondary electron emission caused by the primary electrons colliding with the device wall. It is interesting to note that the number density of the hot population drops slightly as the primary electron energy is increased, even though in isolation the increased primary electron energy should result in increased numbers of secondary electrons. We believe that the reason for this behavior is that the decrease in the number density of isotropic primary electrons with filament bias decreases SEE and keeps the secondary electrons to a roughly constant number density, between 1.3 x 10^{12} and 2.1 x 10^{12} m^{-3}. The number density of the directed beam of electrons decreases as filament bias is increased, though not as rapidly as the isotropic population.

When the filament bias is increased from -70 V to -200 V, the cold electron population increases to a maximum number density of 2.1 x 10^{12} m^{-3} at -120 V, and then decreases to 7.2 x 10^{11} m^{-3} at -200 V. The decrease at highly-negative filament bias is probably due to the loss of magnetic confinement of the primary electrons evident in the disappearance of the isotropic energetic population, as well as the decreased argon ionization cross section at relative energies greater than ~70 eV. Temperature trends are shown in Figure 5, revealing an increase in the plasma temperatures over the smooth sample when the filament is driven below -100 V. Using the harmonic mean of the hot and cold electron temperatures, the Debye length is calculated to range between 3 and 6 mm.

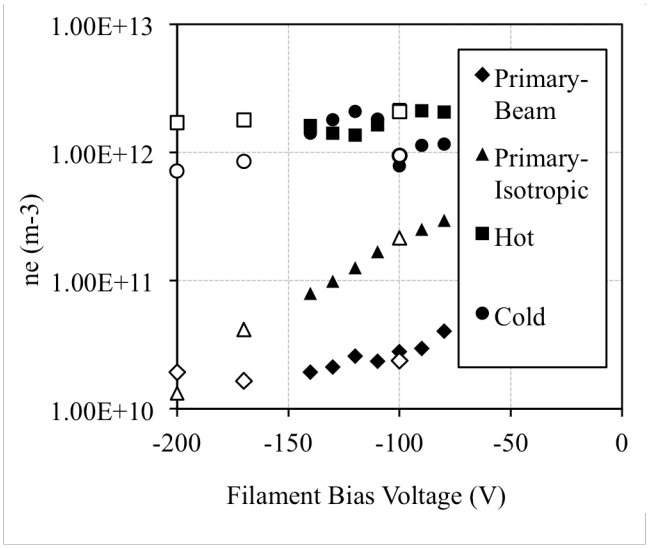

Figure 6. Electron densities measured by Langmuir probe for varied bias of the discharge filament. *Discharge current is 10 mA. Filled symbols are taken with smooth BN sample facing the discharge filament, open symbols with rough BN sample.*

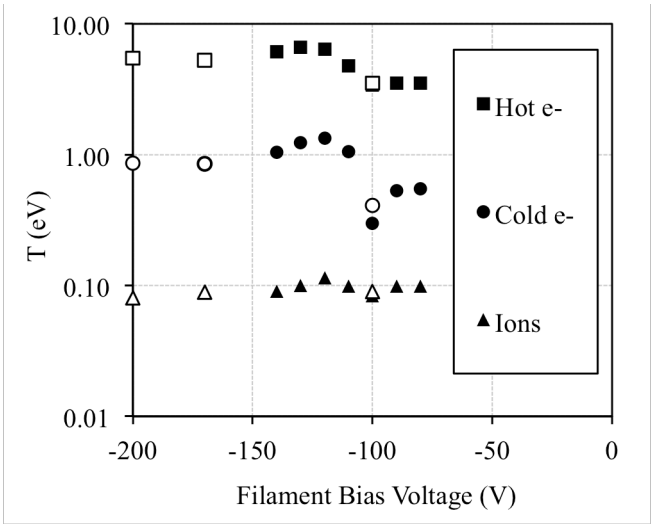

Figure 5. Temperatures measured by Langmuir probe for varied bias of the discharge filament. *Discharge current is 10 mA. Filled symbols are taken over smooth BN sample facing the discharge filament, open symbols over rough BN sample.*

B. Sheaths

Figure 7 shows the experimentally measured plasma potential (V_p) profiles over the rough and smooth BN wall material samples for a range of filament biases. The profiles are presented with respect to the bulk plasma potential (defined as the plasma potential measured 100 mm from the wall in each case.)

Initially, as filament bias is driven more negative, the sheath potential fall increases in order to repel enough off-normal isotropic primary electrons to enforce zero net current to the electrically isolated wall. However, once the filament bias passes a certain threshold, the SEE from the boron nitride wall becomes too great to sustain a large potential fall. Once the potential barrier of the sheath is weakened by SEE, more energy is imparted to the wall by the primary electrons, increasing SEE, and the sheath abruptly changes to a new equilibrium. The potential fall

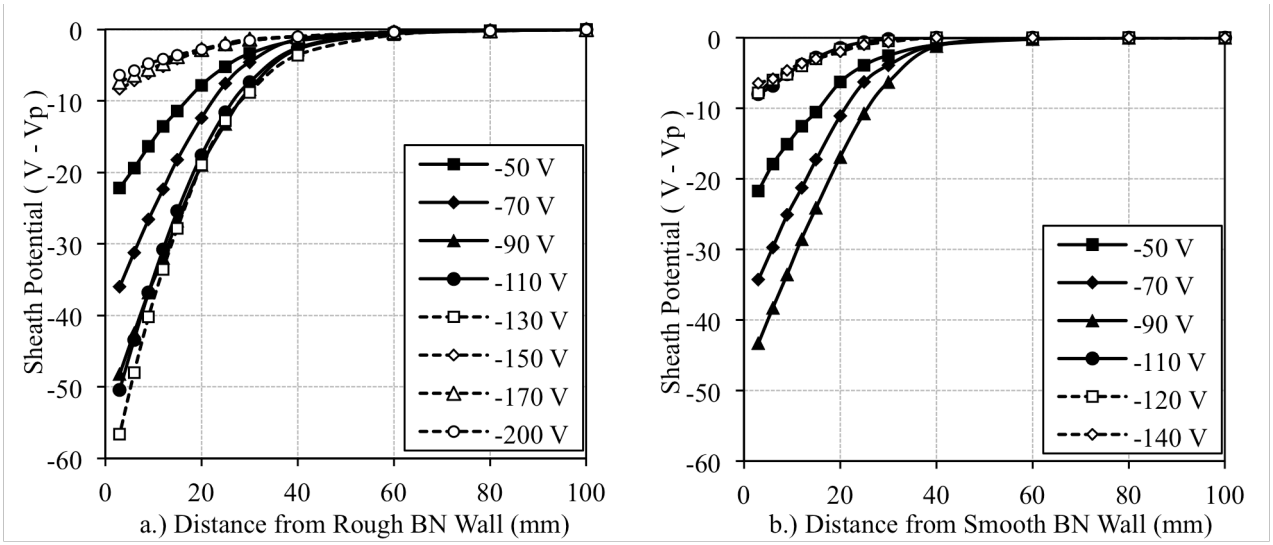

Figure 7. Experimentally measured plasma potential profiles in the sheath over the a.) rough (R_a = 10.4 µm) and b.) smooth (R_a < 0.2 µm) BN wall material samples for different negative biases of the discharge filaments. *Potentials are with respect to the sheath edge potential as measured at 100 mm.*

becomes the order of the electron temperature of the hot secondary electron population. Further increases in primary electron energy continue to decrease the sheath potential.

The collapsed sheath profiles seem similar to the well known space-charge-limited sheath profile predicted by Hobbs and Wesson[20]. Although the sheath potential assumes a value of ~T_e as predicted by the Hobbs and Wesson solution, any relative agreement is not expected to be meaningful because the situations considered are different: in the Hobbs and Wesson case, emission is driven by a plasma at a single equilibrium T_e, whereas the current sheath transition is caused by a scarce energetic population above a denser, cooler plasma.

In addition to the Hobbs and Wesson profile, recent predictions have shown that the sheath potential profile may continue to collapse and reverse in polarity, such that the wall is at a higher potential than the plasma[21]. These sheaths have been referred to as inverse sheaths. The condition for these sheaths to appear is roughly that the SEE yield from the wall must become greater than unity. We expect that we do not achieve yield greater than unity for the hot and cold electron populations, which outnumber the energetic primaries and keep the overall yield less than unity in the collapsed sheath cases.

The sheaths over the rough and the smooth samples are similar within the measurement precision, except that the sheath over the smooth sample transitions to the collapsed equilibrium at a lower filament bias than the sheath over the rough sample. This provides additional evidence that SEE is the driving factor in precipitating the sheath transition, as it is known that a roughened surface will trap candidate secondary electrons that could otherwise escape and thus decrease the overall SEE yield.

As the samples are heated to 400 °C and 600 °C, the voltage at which the sheath collapse occurs shifts to a higher value for the rough samples, but remains mostly unchanged for the smooth samples. This is shown in Figure 8. This result could be due in large part to evaporation of contaminants from the sample surface, which is known to affect SEE in this way[22]. Experiments are ongoing to determine if this effect is only due to the evaporation of contaminants from the sample surface, or

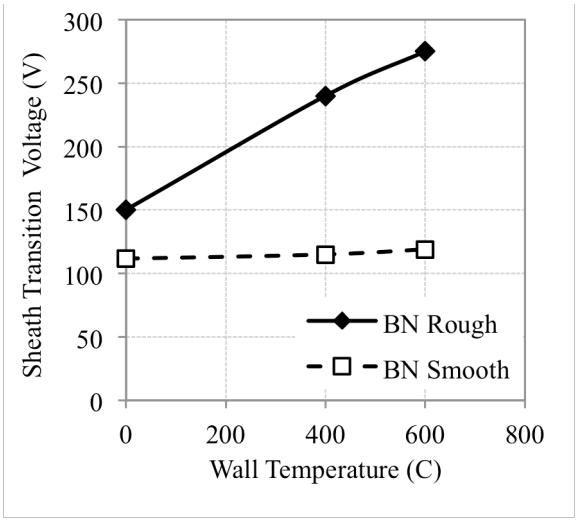

Figure 8. Filament bias voltage at which sheath transition occurs vs. wall temperature. *Experiments performed from cold to hot temperatures. Experiments are ongoing to determine if effects persist after a heating-cooling cycle.*

if there is a decoupled effect of the surface temperature.

IV. Conclusions

A new set of experimental results is provided for the case of a floating wall, a non-thermal plasma, and significant secondary electron emission. A transition in the sheath structure similar to the space-charge-limited sheath predicted by Hobbs and Wesson is observed, however the conditions that lead to the transition are different. Comparison of the measurements with roughened and smooth samples shows that the sheaths are very similar when in the same sheath regime (far from the transition condition,) but also shows that the smooth wall material samples transition at lower incident electron energies than the rough samples. As well as providing confirmation that SEE is the driving factor behind the observations, the result suggests that control of surface finish could provide a means of avoiding or precipitating sheath transitions driven by SEE. The results have implications for thruster plasmas in which the bounding surfaces are modified by ion sputtering, namely that a gradually occurring change in the surface structure could facilitate a sudden transition in the sheath structure and thus a sudden deviation from the designed operation.

Acknowledgments

The authors would like to thank Thomas Burton and Aaron Schinder for their assistance in procurement, preparation and characterization of the material samples used in this work. This work is supported by the Air Force Office of Scientific Research through Grant FA9550-11-10160.

References

[1]Langendorf, S., Walker, M. L.R., Rose, L., Keidar, M., Brieda, L., Effect of Ion-Neutral Collisions on Sheath Potential Profile. In 33rd International Electric Propulsion Conference, IEPC-2013-346, Washington DC, USA.

[2]Langendorf, S., Walker, M. L. R., Rose, L., Keidar, M., Brieda, L., Study of the Plasma-Wall Interface – Measurement and Simulation of Sheath Potential Profiles. In 49th AIAA/ASME/SAE/ASEE Joint Propulsion Conference (JPC), San Jose CA, USA.

[3]Viel-Inguimbert, V. (2003, March). Secondary electron emission of ceramics used in the channel of SPT. In 28th International Electric Propulsion Conference, IEPC-2003-258, Toulouse, France.

[4]Private communication with M. Keidar, May 2014.

[5]Oksuz, L., and Hershkowitz, N. "Plasma, presheath, collisional sheath and collisionless sheath potential profiles in weakly ionized, weakly collisional plasma." *Plasma Sources Science and Technology* 14.1 (2005): 201.

[6]Lee, D., Severn, G., Oksuz, L., and Hershkowitz, N. "Laser-induced fluorescence measurements of argon ion velocities near the sheath boundary of an argon–xenon plasma." *Journal of Physics D: Applied Physics*, 39(24), (2006): 5230.

[7]Limpaecher, Rudolf; Mackenzie, K.R., "Magnetic Multipole Containment of Large Uniform Collisionless Quiescent Plasmas," *Review of Scientific Instruments*, vol. 44, no. 6, pp. 726-731, June (1973).

[8]Lang, A. and Hershkowitz, N. "Multidipole plasma density." *J. Appl. Phys*. 49, 4707 (1978).

[9]Langendorf, S. J., Walker, M. L. R., Rose, L., Keidar, M., Brieda, L., AIAA 2013-4128. *Proceedings of the 49th AIAA/ASME/SAE/ASEE Joint Propulsion Conference*, "Wall Material Effects on Sheath Potential Profile." San Jose, CA, July 14 - 17, (2013).

[10]Kieckhafer, A. W., and Walker, M. L. R., *Proceedings of the 32nd International Electric Propulsion Conference*, "Recirculating Liquid Nitrogen System for Operation of Cryogenic Pumps", Hamburg, Germany, September (2011).

[11]Stanford Research Systems, Appl. Note "Bayard-Alpert Ionization Gauges", pp. 38, <http://www.thinksrs.com/downloads/PDFs/ApplicationNotes/IG1BAGapp.pdf> [cited 1 July 2013].

[12]Walker, M. L., Keidar, M., Ready, W. J., Rimoli, J. J., & Thompson, G. (2012). *Comprehensive Study of Plasma-Wall Sheath Transport Phenomena,* OMB No. 0704-0188 2012. September 10, 2012, Arlington, VA.

[13]Sheehan, J. P., et al. "A comparison of emissive probe techniques for electric potential measurements in a complex plasma." *Physics of Plasmas* 18 (2011): 073501.

[14]Hagstrum, H. D. "Theory of Auger ejection of electrons from metals by ions." *Physical Review*, 96(2), 336 (1954).

[15]Chaudhri, R. M. (1941). "Secondary Electron Emission From Tungsten." In *Proceedings of the National Institute of Sciences of India* (Vol. 7, p. 197). National Institute of Sciences of India.

[16]Allen, J. E. (1992). Probe theory-the orbital motion approach. *Physica Scripta*, 45(5), 497.

[17]Hershkowitz, N., DeKock, J. R., Coakley, P., & Cartier, S. L. (1980). "Surface trapping of primary electrons by multidipole magnetic fields." *Review of Scientific Instruments*, 51(1), 64-69.

[18]Stamate, E., Inagaki, K., Ohe, K., & Popa, G. (1999). "On energetic electrons in a multipolar magnetically confined Ar plasma." *Journal of Physics D: Applied Physics*, 32(6), 671.

[19]Robertson, S., Knappmiller, S., & Sternovsky, Z. (2006). "Energy balance and plasma potential in low-density hot-filament discharges." *IEEE Transactions on Plasma Science*, 34(3), 844-849.

[20]Hobbs, G. D., & Wesson, J. A. (1967). Heat flow through a Langmuir sheath in the presence of electron emission. *Plasma Physics*, 9(1), 85.

[21]Campanell, M. D. (2013). Negative plasma potential relative to electron-emitting surfaces. Physical Review E, 88(3), 033103.

[22]Chaudhri, R. M. (1941). Secondary Electron Emission from Tungsten. In Proceedings of the National Institute of Sciences of India (Vol. 7, p. 197). National Institute of Sciences of India.